Journal of Inorganic Biochemistry 195 (2019) 141–148

Contents lists available at ScienceDirect

Journal of Inorganic Biochemistry

journal homepage: www.elsevier.com/locate/jinorgbio

Formation and stability of the mixed-chelator complexes of Sr^{2+}, Mg^{2+}, Ca^{2+}, Ba^{2+}, and Y^{3+} in solution with bio-relevant chelators

Zinnat A. Begum[a,b,*,1], Ismail M.M. Rahman[c,*,1], Tsugiko Takase[c], Hiroshi Hasegawa[d,*]

[a] Venture Business Laboratory, Organization of Frontier Science and Innovation, Kanazawa University, Kakuma, Kanazawa 920-1192, Japan
[b] Department of Civil Engineering, Southern University, 739/A Mehedibag Road, Chittagong 4000, Bangladesh
[c] Institute of Environmental Radioactivity, Fukushima University, 1 Kanayagawa, Fukushima City, Fukushima 960-1296, Japan
[d] Institute of Science and Engineering, Kanazawa University, Kakuma, Kanazawa 920-1192, Japan

ARTICLE INFO

Keywords:
Ternary complexation
Divalent and trivalent ions
Biodegradable chelator
Equilibrium constant

ABSTRACT

The formation and equilibria of Sr^{2+}, Mg^{2+}, Ca^{2+}, Ba^{2+}, and Y^{3+} (M) complexes with a mixed-chelator comprising two biodegradable chelators (GLDA, L_G, 2-[bis(carboxymethyl)amino] pentanedioic acid; HIDS, L_H, 2-(1,2-dicarboxyethylamino)-3-hydroxy-butanedioic acid) in an aqueous matrix was evaluated. The potentiometric measurement results (ionic strength, 0.10 M; temperature, 25 ± 0.1 °C) confirmed the formation of 1:1:1 ($M:L_G:L_H$) complexes and the experimental data sets were further used to derive the equilibrium constants for the ternary complexes. The $[MHL_GL_H]^{5-}$ complex was the dominant ternary complex with Sr^{2+}, Mg^{2+}, Ca^{2+}, and Ba^{2+}, while Y^{3+} formed $[M(OH)_2L_GL_H]^{7-}$ as the principal ternary species. The trend in the overall formation constants of the ML_{mix} (L_{mix}, $L_G:L_H$ = 1:1) complexes was in the order: $Y^{3+} > Ca^{2+} > Mg^{2+} > Sr^{2+} > Ba^{2+}$. The ternary complexation trend was interpreted using the corresponding atomic radii and solution-phase electronegativities of the elements. The modes of interaction between the chelators and cations in the ML_{mix} systems were subsequently deduced, and evaluated by using Gaussian 16W program. The relative stabilities of the ternary complexes ($\Delta \log K$) were interpreted by comparison with the stabilities of the corresponding binaries, with negative $\Delta \log K$ values observed for all the ML_{mix} complexes.

1. Introduction

Radiostrontium (r-Sr) is one of the most commonly measured radioelements in environmental radioactivity monitoring [1]. The ecosystem receives r-Sr (^{90}Sr, ^{89}Sr, ^{85}Sr) from nuclear technology-related activities and uncharacteristic emissions following nuclear incidents [2]. The healthcare, research, and industrial sectors also use r-Sr to exploit beta emission energy [3]. The intrusion of r-Sr in the biosphere evokes concern because of its higher mobility over that of many other radioelements [4] and a propensity of the residual r-Sr to remain in the upper soil layer (≤10 cm) [5,6]. The r-Sr ions (Sr^{2+}) accumulate in bone and bone marrow and can cause bone cancer, leukemia, and cancer of the adjacent soft tissue [7,8].

Chelators, which can bind with metals to create stable complexes [9], are commonly used in nuclear facility decontamination activities [10], treatment of radiation sickness [11], and washing remediation of radionuclide-contaminated solids [12]. The use of chelators is favored in solid-waste treatment due to broad-range applicability and suitable economics [13–15]. Nevertheless, the after-use environmental release of classical chelators, such as EDTA (2,2′,2″,2‴-(ethane-1,2-diyldinitrilo)tetraacetic acid), DTPA (2-[bis[2-[bis(carboxymethyl) amino] ethyl]amino]acetic acid), and their homologs, is criticized due to the endless persistence in the environment and subsequent lethal exposure of these compounds [9,16]. Biodegradable alternatives to classical chelators, including EDDS (2-[2-(1,2-dicarboxyethylamino) ethylamino]butanedioic acid), GLDA (2-[bis(carboxymethyl)amino]pentanedioic acid), HIDS (2-(1,2-dicarboxyethylamino)-3-hydroxy-butanedioic acid), IDSA (2-(1,2-dicarboxyethyl amino)butanedioic acid), MGDA (2-[bis(carboxymethyl)amino]propanoic acid), have thus been introduced [13,17,18].

Our research interest is the exploration of the potential of new biodegradable chelators for solid-waste processing applications. Thus, our earlier works include studies on 1:1 metal-chelator complex formation characteristics [19–21] and their impact on washing

* Corresponding authors.
E-mail addresses: zinnat.ara@staff.kanazawa-u.ac.jp (Z.A. Begum), immrahman@ipc.fukushima-u.ac.jp (I.M.M. Rahman), hhiroshi@se.kanazawa-u.ac.jp (H. Hasegawa).
[1] Co-first author.

https://doi.org/10.1016/j.jinorgbio.2019.03.018
Received 7 January 2019; Received in revised form 19 March 2019; Accepted 19 March 2019
Available online 22 March 2019
0162-0134/

remediation and rare-element recovery from solid wastes [12,22–25]. The formation, stability, and bioavailability of metal-chelator complexes are conventionally assumed in view of 1:1 binary complexation under equilibrium conditions [26]. However, interactions between multi-chelator and multi-element ions commonly occur in biological and environmental conditions to generate mixed-chelator or higher-order complexes [27]. Ternary complexes, the simplest of such higher-order complexes consisting of one metal ion and two different chelators, are essential to explore the ion binding potential in, among others, pharmaceutical and biotechnological applications [28–33]. Moreover, better element-extractability of mixed chelators comprising EDTA and organic chelators (e.g., oxalate, GLDA, and citric acid) from solid wastes has been reported [34,35].

As a continuation of our research on the complexation behavior of biodegradable chelators with ecologically important ions, herein we present a study of the ternary complexes of Sr^{2+}, Mg^{2+}, Ca^{2+}, Ba^{2+}, and Y^{3+} with GLDA and HIDS (ionic strength, $I = 0.10$ M; temperature, $T = 25$ °C). Other ions (Mg^{2+}, Ca^{2+}, Ba^{2+}, and Y^{3+}) have been included with Sr^{2+} due to their biochemical likeness (Ca^{2+}) [7,8] or similarity in geochemical features (Mg^{2+} and Ba^{2+}) [36,37], while Y^{3+}, which exists in secular equilibrium in the environment, is the daughter-isotope of r-Sr [1]. Further, GLDA and HIDS were selected as an alternative to classical chelators, e.g., EDTA and its homologs, for their biodegradability and superior complexation ability over those of the frequently-recommended green EDTA-alternatives, e.g., EDDS [19] and IDSA [21]. In this study, the stable Sr-isotopes (^{84}Sr, ^{86}Sr, and ^{88}Sr) are used as a natural analog to r-Sr since their resemblance in biogeochemical features is conforming [38]. The newly derived data-sets show great potential for application in the washing decontamination of residuals from nuclear energy-related activities containing r-Sr and its geochemically-related elements.

2. Experimental

2.1. Instrumentation

A KEM AT-710 automatic titrator (Kyoto Electronics, Kyoto, Japan) was used for the potentiometric measurements. The titration system included a pH-combination electrode, temperature probe, dosing nozzle connected to a titrator, magnetic stirrer, and titration vessel. The 100 mL titration vessel comprised an inlet and outlet for N_2 gas-flow as well as inlets for each of the abovementioned components.

An SKG-01 heat exchanger bath (AS ONE, Tokyo, Japan) was combined to a TBK202HA constant temperature water heater (Advantec, Tokyo, Japan) and Eyela CTP-1000 thermo-controlled water circulator (Tokyo Rikakikai, Tokyo, Japan) to maintain controlled-temperature conditions in the solutions.

A PureLab Ultra-Analytic water purification system (ELGA Lab Water, Celle, Germany) was used to produce ultrapure water with a resistivity of > 18 mΩ·cm and total organic content of < 1 μg·dm^{-3}.

A Nexion 350S ICP-MS (inductively coupled plasma mass spectrometer) (Perkin Elmer, Shelton, CT, USA) was used to quantify the metal concentration in the working solutions. The TOSOH 8020 high-performance liquid chromatography system (TOSOH, Tokyo, Japan) was used to validate the chelator concentration in the solutions.

2.2. Biodegradable chelators

The biodegradable chelators GLDA (L_G, $C_9H_{13}NO_8$) (Tokyo Kasei Kogyo, Tokyo, Japan) and HIDS (L_H, $C_8H_{11}NO_9$) (Nippon Shokubai, Tokyo, Japan) (Fig. 1) were used as components in the L_{mix} (L_G + L_H, 1:1) solution. The commercially-available packages of L_G and L_H comprised 40 and 50 wt% solutions, respectively, of the corresponding tetra-sodium salts in the aqueous matrix.

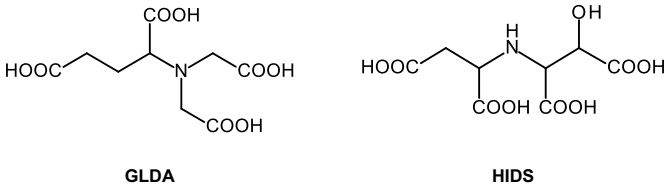

Fig. 1. Chemical structures of the component biodegradable chelators (GLDA, L_G, 2-[bis(carboxymethyl)amino] pentanedioic acid and HIDS, L_H, 2-(1,2-dicarboxyethylamino)-3-hydroxy-butanedioic acid) in the ML_{mix} system.

2.3. Reagents

All the reagents used were of analytical grade and used without further purification. Potassium hydroxide (KOH, CO_2-free), potassium nitrate (KNO_3), and nitric acid (HNO_3) were purchased from Kanto Chemical (Tokyo, Japan) and used as the titrant, background electrolyte, and source of protons in the titer, respectively. The KOH titrant concentration was confirmed using potassium hydrogen phthalate. Standard solutions of pH 4.0, 7.0, and 9.0 (Horiba 101-S, Kyoto, Japan) were used as the calibrants to standardize the electrode prior to the pH-metric experiments as per manufacturer-recommended protocol.

Anhydrous strontium nitrate, magnesium nitrate hexahydrate, yttrium nitrate tetrahydrate (Merck KGaA, Darmstadt, Germany) together with calcium nitrate tetrahydrate and barium nitrate (Wako Pure Chemical, Osaka, Japan), all with a mass fraction purity ≥ 99.9, were dissolved in an aqueous matrix to prepare respective stock solutions of Sr^{2+}, Mg^{2+}, Y^{3+}, Ca^{2+}, and Ba^{2+}. The concentrations of these stock solutions were further verified via ICP-MS measurements. The source standards for ICP-MS were prepared from certified solutions of Sr, Mg, Ca, Ba, and Y (1000 mg·dm^{-3}; SpecCertiPrep, Metuchen, NJ, USA). All the reagents were diluted by mass in the range μmol L^{-1}–mmol L^{-1} using ultrapure water before use.

2.4. Methods

2.4.1. Equilibrium titration

The pH-metric titration data were recorded, using the titrator software, at a pre-set dosing interval (120 s) for each 0.02 mL titrant (KOH, 0.1 M) addition in 50 mL titer. The titer solution comprised the chelators (L_G, L_H, or an equimolar mix of L_G and L_H; 1.0×10^{-3} M), proton-supplier (HNO_3; 1.0×10^{-2} M), metal ions (Sr^{2+}, Mg^{2+}, Ca^{2+}, Ba^{2+}, or Y^{3+}; equimolar ratio to the chelators), and background electrolyte (KNO_3; $I = 0.1$ M). The titer solution was continuously stirred to ensure thorough mixing of the components. An uninterrupted N_2 flow created an inert reaction environment and eliminated the ingress of CO_2 in the titer. The experiment was performed at $T = 25$ °C (uncertainty, ± 0.1 °C). The variation in the titer solution pH with titrant addition was measured using a pre-calibrated electrode up to the third decimal place of pH units (precision, ± 0.001). The incremental addition of the titrant to the titer was continued to produce a real-time titration curve in the solution pH range 2.1–11.2 and the average time leg for each titration was 14 ± 2 h. The titrations were initiated from the acid region as the solution homogeneity was presumably higher at lower pH values [39]. Each titration was repeated at least fivefold and the computational analysis used ≥150 pH data points.

2.4.2. Data processing

GLEE 3.0 [40], HySS2009 [41], and Hyperquad2008 [42] software programs were used to process the experimental potentiometric data-sets (Table S1, Appendix A: Supplementary information).

The GLEE (Glass electrode evaluation) program computed the impact of the electrode junction potentials on the measured pH values at low and high pH regions based on the strong acid-base titration results. The objective was to estimate the extent of carbonate contamination in

the base solution, electrode potential, and slope factor (hydrolysis constant of water, $pK_w = 13.79$, $I = 0.1$ M, $T = 25$ °C). The uncertainty in the meter reading was < 0.05 mV.

The HySS (Hyperquad simulation and speciation) program was used to simulate the titration requirements that support the pre-assumed model representing the chemical equilibria in the solution obtained using mass-balance equations. The equilibrium model and experimental potentiometric data were then entered into the Hyperquad program to estimate the metal-chelator complexation constants using a non-linear refinement technique. The estimate was further improved by the interactive adjustment of the model to obtain a reasonably good fit, which only presented small systematic trends in the residuals between the observed and calculated values. The protonation constants for L_G and L_H (Table S2; Appendix A: Supplementary information) [21] and the hydrolysis constants of the Sr^{2+}, Mg^{2+}, Ca^{2+}, Ba^{2+}, and Y^{3+}species (Table S3; Appendix A: Supplementary information) [43] were added as invariable parameters to the Hyperquad2008 program to facilitate the programmed-correction of the complexation constants that were calculated as variables.

Gaussian 16W [44] was used to perform the density functional theory (DFT) calculations of isolated L_G and L_H molecules and the corresponding ternary M^{2+} (Sr^{2+}, Mg^{2+}, Ca^{2+}, and Ba^{2+}) complexes, which were optimized using the B3LYP method. The LanL2DZ basis set was used for M^{2+}-atoms while 6-31 G(d) basis set was employed for C, N, O, and H, which were combined with the CPCM solvation method (solvent, H_2O).

3. Results and discussion

3.1. Formation of the ternary complexes

The protonation of the chelators during the pH-metric titrations in the absence of metal ions, β_n, was calculated using the overall reaction:

$$\beta_n = K_{a1}\cdot K_{a2}\cdots K_n = \frac{[H_nL]}{[H]^n[L]} \quad (1)$$

where K_{a1}, K_{a2}… K_n represent the stepwise acid dissociation constants; [H] represents the protons associated with the chelators; and [L] represents the L_G and L_H contents in solution. The previously reported pK_a values for L_G (9.39, 5.01, 3.49, 2.56) and L_H (9.61, 4.07, 3.08, 2.14), $T = 25$ °C; $I = 0.1$ M [21], indicate that the protonations occur at the amino nitrogen and carboxyl oxygen positions. The protonation equilibria of L_G and L_H are presented in Table S2 (Appendix A: Supplementary information).

The best composition model was selected to calculate the formation constants ($\log_{10}\beta_{pqrs}$) for the ternary complexes of Sr^{2+}, Mg^{2+}, Ca^{2+}, Ba^{2+}, and Y^{3+} with the L_G and L_H mixed solution in the aqueous matrix (Table 1). The determining factors were the consistency between the predicted and experimental potentiometric data, best statistical fit, and relevance to the chemical approach. The overall stoichiometry associated with the possible equilibria in the mixed-chelator (ML_{mix}) system can be expressed by the equation:

$$pM + qH + rL_G + sL_H \leftrightharpoons M_pH_qL_{Gr}L_{Hs} \quad \beta_{pqrs} = \frac{[M_pH_qL_{Gr}L_{Hs}]}{[M]^p[H]^q[L_G]^r[L_H]^s} \quad (2)$$

where the symbols p, q, r, and s represent the respective stoichiometric coefficients for the metal ions (M = Sr^{2+}, Mg^{2+}, Ca^{2+}, Ba^{2+}, and Y^{3+}), [H], L_G, and L_H in the ML_{mix} system under equilibrium conditions.

The coordination of two different chelators (L_G and L_H) with M (Sr^{2+}, Mg^{2+}, Ca^{2+}, Ba^{2+}, and Y^{3+}) can be expressed by Eqs. (3)–(8) to define the stepwise formation constant ($\log_{10}K$) in the ML_{mix} systems:

$$M + L_G \leftrightharpoons ML_G \quad K_{ML_G} = \frac{[ML_G]}{[M][L_G]} \quad (3)$$

$$M + L_H \leftrightharpoons ML_H \quad K_{ML_H} = \frac{[ML_H]}{[M][L_H]} \quad (4)$$

$$ML_G + L_H \leftrightharpoons ML_GL_H \quad K_{ML_GL_H} = \frac{[ML_GL_H]}{[ML_G][L_H]} \quad (5)$$

$$ML_H + L_G \leftrightharpoons ML_HL_G \quad K_{ML_HL_G} = \frac{[ML_HL_G]}{[ML_H][L_G]} \quad (6)$$

$$ML_GL_H + H^+ \leftrightharpoons MHL_GL_H \quad K_{MHL_GL_H} = \frac{[MHL_GL_H]}{[ML_GL_H][H]} \quad (7)$$

$$ML_HL_G + H^+ \leftrightharpoons MHL_HL_G \quad K_{MHL_HL_G} = \frac{[MHL_HL_G]}{[ML_HL_G][H]} \quad (8)$$

The coordination of the water molecules involves additional deprotonation reactions in the ML_{mix} systems and can be defined as:

$$ML_GL_H(H_2O) \leftrightharpoons M(OH)L_GL_H + H^+ \quad K_{M(OH)L_GL_H} = \frac{[M(OH)L_GL_H][H]}{[ML_GL_H(H_2O)]} \quad (9)$$

$$ML_HL_G(H_2O) \leftrightharpoons M(OH)L_HL_G + H^+ \quad K_{M(OH)L_HL_G} = \frac{[M(OH)L_HL_G][H]}{[ML_HL_G(H_2O)]} \quad (10)$$

The ML_{mix} complexes, namely ML_GL_H and ML_HL_G (Eqs. (5) and (6), respectively), MHL_GL_H and MHL_HL_G (Eqs. (7) and (8), respectively), and $M(OH)L_GL_H$ and $M(OH)L_HL_G$ (Eqs. (9) and (10), respectively) act identically when they remain labile in solution [45].

The titration curves for the formation of the ternary complexes in the ML_{mix} system containing 1:1:1 stoichiometric mixtures of M:L_G:L_H were then compared to those obtained for the protonations of L_G and L_H and a 1:1 binary mixture of M:L_G and M:L_H, respectively (Figs. 2a, 3a, 4a, 5a, and 6a). The complexation characteristics of the M:L_G and M:L_H binary systems under similar conditions have been reported by Begum et al. [19]. The compared theoretical and experimental titration data for the ML_{mix} system (M:L_G:L_H, 1:1:1), illustrated in the insets of Figs. 2a, 3a, 4a, 5a, and 6a, are limited to the complexation zone to ensure better visualization. The theoretical and experimental titration curves are almost overlapped thereby confirming the validity of the assumed complexation models. The deviations in the titration curves for M:L_G:L_H compared to those of the binary M:L_G and M:L_H samples confirmed the occurrences of ternary complexation in the ML_{mix} system, while the inflection at higher pH values indicated the presence of metal-hydroxy species [46].

Refinements over the entire pH range were converged successfully for the M + L_G + L_H (1:1:1) composition, while the following complexation equilibria were terminated: $(M)_2$ + L_G + L_H (2:1:1). Moreover, the presence of $M(L_G)_2$ or $M(L_H)_2$ species in the 1:2 binary systems (M = Sr^{2+}, Mg^{2+}, Ca^{2+}, Ba^{2+}, and Y^{3+}) was not validated [19].

The formation of ternary complexes via the equimolar binding of two different chelators with the metal ions is straightforward. However, it might also occur via a complete 1:1 complexation between M and L_G or L_H to form the respective ML_G or ML_H complex in the first step, followed by a subsequent 1:1 complexation of ML_G or ML_H with L_H or L_G [47,48]. In general, the chelating potential of L_G and L_H determines whether the complex formation mechanism is stepwise or simultaneous [26].

3.2. Speciation of the ternary complexes

A statistical assumption predicted 50% ternary complex formation in the ML_{mix} system and ≤25% binary parent complex formation [49]. The complexation of metal (M = Sr^{2+}, Mg^{2+}, Ca^{2+}, Ba^{2+}, and Y^{3+}) with the L_G and L_H mix was characterized by the formation of 1:1:1 (M:L_G:L_H) complexes and 1:1 complexes of M:L_G and M:L_H, which were dominant in the ML_{mix} system.

Table 1
The overall formation constants ($\log_{10}\beta_{pqrs}$) for the ternary ML_{mix} complexes (M = Sr^{2+}, Mg^{2+}, Ca^{2+}, Ba^{2+}, or Y^{3+}; L_{mix} = L_G + L_H, L_G, GLDA and L_H, HIDS)[a,b].

Formation reactions	*p*	*q*	*r*	*s*	$\log_{10}\beta_{pqrs}$	SD
Sr^{2+}						
$Sr^{2+} + L_G^{4-} + L_H^{4-} \rightleftharpoons [SrL_GL_H]^{6-}$	1	0	1	1	7.67	0.04
$Sr^{2+} + H^+ + L_G^{4-} + L_H^{4-} \rightleftharpoons [SrHL_GL_H]^{5-}$	1	1	1	1	17.44	0.02
$Sr^{2+} + 2H^+ + L_G^{4-} + L_H^{4-} \rightleftharpoons [SrH_2L_GL_H]^{4-}$	1	2	1	1	25.17	0.01
Mg^{2+}						
$Mg^{2+} + OH^- + L_G^{4-} + L_H^{4-} \rightleftharpoons [Mg(OH)L_GL_H]^{7-}$	1	–1	1	1	−1.18	0.02
$Mg^{2+} + L_G^{4-} + L_H^{4-} \rightleftharpoons [MgL_GL_H]^{6-}$	1	0	1	1	9.08	0.03
$Mg^{2+} + H^+ + L_G^{4-} + L_H^{4-} \rightleftharpoons [MgHL_GL_H]^{5-}$	1	1	1	1	18.67	0.02
$Mg^{2+} + 2H^+ + L_G^{4-} + L_H^{4-} \rightleftharpoons [MgH_2L_GL_H]^{4-}$	1	2	1	1	25.1	0.01
Ca^{2+}						
$Ca^{2+} + OH^- + L_G^{4-} + L_H^{4-} \rightleftharpoons [Ca(OH)L_GL_H]^{7-}$	1	−1	1	1	−0.78	0.01
$Ca^{2+} + L_G^{4-} + L_H^{4-} \rightleftharpoons [CaL_GL_H]^{6-}$	1	0	1	1	9.43	0.01
$Ca^{2+} + H^+ + L_G^{4-} + L_H^{4-} \rightleftharpoons [CaHL_GL_H]^{5-}$	1	1	1	1	18.92	0.02
$Ca^{2+} + 2H^+ + L_G^{4-} + L_H^{4-} \rightleftharpoons [CaH_2L_GL_H]^{4-}$	1	2	1	1	24.95	0.01
Ba^{2+}						
$Ba^{2+} + OH^- + L_G^{4-} + L_H^{4-} \rightleftharpoons [Ba(OH)L_GL_H]^{7-}$	1	−1	1	1	−3.57	0.04
$Ba^{2+} + L_G^{4-} + L_H^{4-} \rightleftharpoons [BaL_GL_H]^{6-}$	1	0	1	1	7.17	0.02
$Ba^{2+} + H^+ + L_G^{4-} + L_H^{4-} \rightleftharpoons [BaHL_GL_H]^{5-}$	1	1	1	1	16.83	0.02
$Ba^{2+} + 2H^+ + L_G^{4-} + L_H^{4-} \rightleftharpoons [BaH_2L_GL_H]^{4-}$	1	2	1	1	24.9	0.01
Y^{3+}						
$Y^{3+} + 3OH^- + L_G^{4-} + L_H^{4-} \rightleftharpoons [Y(OH)_3L_GL_H]^{8-}$	1	−3	1	1	4.55	0.02
$Y^{3+} + 2OH^- + L_G^{4-} + L_H^{4-} \rightleftharpoons [Y(OH)_2L_GL_H]^{7-}$	1	−2	1	1	14.46	0.02
$Y^{3+} + OH^- + L_G^{4-} + L_H^{4-} \rightleftharpoons [Y(OH)L_GL_H]^{6-}$	1	−1	1	1	20.61	0.01
$Y^{3+} + L_G^{4-} + L_H^{4-} \rightleftharpoons [YL_GL_H]^{5-}$	1	0	1	1	25.26	0.01
$Y^{3+} + H^+ + L_G^{4-} + L_H^{4-} \rightleftharpoons [YHL_GL_H]^{4-}$	1	1	1	1	28.84	0.02
$Y^{3+} + 2H^+ + L_G^{4-} + L_H^{4-} \rightleftharpoons [YH_2L_GL_H]^{3-}$	1	1	1	1	32.56	0.01

[a] I = 0.1 M; T = 25 °C; M:L_G:L_H = 1:1:1; matrix, H_2O.
[b] Experimental potentiometric data were processed using Hyperquad2008 to derive the $\log_{10}\beta_{pqrs}$ (n = 3). The symbols *p*, *q*, *r*, and *s* respectively denote the stoichiometric coefficients for Sr^{2+}, Mg^{2+}, Ca^{2+}, Ba^{2+}, or Y^{3+}, proton, L_G, and L_H in the ML_{mix} system associated with the possible equilibria in solution.

The species distribution curves for the ML_{mix} system containing divalent metal ions (M = Sr^{2+}, Mg^{2+}, Ca^{2+}, and Ba^{2+}; L_{mix} = L_G + L_H) suggested that the complexation started in increasing proportions at ~pH 3.3 with the formation of bi-protonated ($[MH_2L_GL_H]^{4-}$), protonated ($[MHL_GL_H]^{5-}$), and deprotonated ($[ML_GL_H]^{6-}$) ternary species (Figs. 2b, 3b, 4b, and 5b). On the other hand, except with Sr^{2+}, the formation of ternary ML_{mix}–hydroxy species ($[M(OH)L_GL_H]^{7-}$) was observed at higher pH values (pH ≥ 9). The dominating formation of $[Sr(OH)L_H]^{3-}$ in the ML_{mix} system (Fig. 2b) was attributed to the higher degree of stability of the binary Sr^{2+}–hydroxy chelates over those of the corresponding ternaries. A similar tendency was also observed for Ba^{2+} with the dominant formation of $[Ba(OH)L_H]^{3-}$ over that of ($[Ba(OH)L_GL_H]^{7-}$; Fig. 5b). The maximum ternary complexation of L_{mix} with the divalent ions occurred in the range 25–41%, while the highest formation rate for the binary complexes ($[ML_G]^{2-}$ and $[ML_H]^{2-}$) was observed in the range 12–42%.

The ternary complexes of Y^{3+} and L_{mix} (L_G + L_H), ($[YH_2L_GL_H]^{3-}$, $[YHL_GL_H]^{4-}$, $[YL_GL_H]^{5-}$, $[Y(OH)L_GL_H]^{6-}$, $[Y(OH)_2L_GL_H]^{7-}$, and $[Y(OH)_3L_GL_H]^{8-}$) started to form at pH < 2, with the highest formation ratio of $[Y(OH)_2L_GL_H]^{7-}$ (95%) observed at the basic pH region (Fig. 6b). The speciation observed for Y^{3+} was significantly different from those observed for the di-cations. The formation of ternary Y^{3+} complexes began at a pH < 2 and was dominant across the whole pH range as compared to binary complex formation. Moreover, the Y^{3+}–hydroxy–L_{mix} chelates largely dominated the speciation diagram at pH > 6, possibly due to the strong hydrolytic behavior of Y^{3+}.

The chelators used in this work contain basic amino nitrogen donor groups that can associate with protons (H^+) in low-to-medium pH

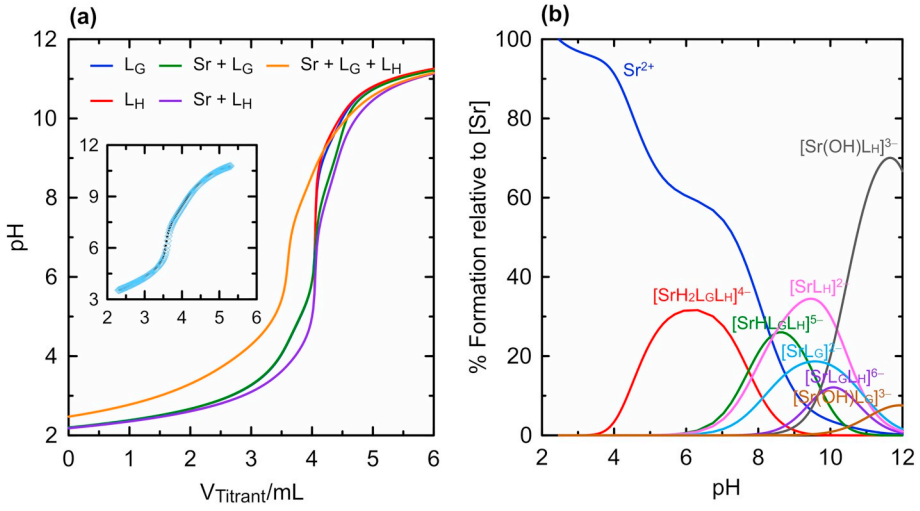

Fig. 2. (a) Real-time potentiometric titration curves for the protonation of L_G and L_H and the formation of the corresponding binary (M:L_G or M:L_H, 1:1) and ternary (M:L_G:L_H, 1:1:1) Sr^{2+} complexes. Inset: comparison of the theoretical (dashed line) and experimental (◊) titration data for the ternary mixtures (M:L_G:L_H, 1:1:1) at the complexation zone of the real-time potentiometric titration curve. (b) Speciation of the Sr^{2+} complexes in the ML_{mix} (L_{mix} = L_G + L_H; M:L_G:L_H, 1:1:1) system (I = 0.1 M; T = 25 °C; matrix, H_2O).

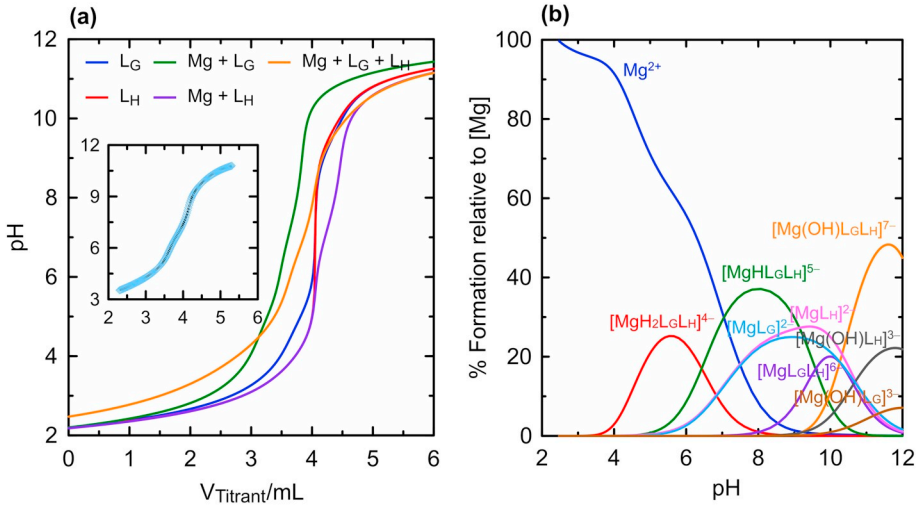

Fig. 3. (a) Real-time potentiometric titration curves for the protonation of L_G and L_H and the formation of the corresponding binary (M:L_G and M:L_H, 1:1) and ternary (M:L_G:L_H, 1:1:1) Mg^{2+} complexes. Inset: comparison of the theoretical (dashed line) and experimental (◊) titration data for the ternary mixtures (M:L_G:L_H, 1:1:1) at the complexation zone of the real-time potentiometric titration curve. (b) Speciation of the Mg^{2+} complexes in the ML_{mix} (L_{mix} = L_G + L_H; M:L_G:L_H, 1:1:1) system (I = 0.1 M; T = 25 °C; matrix, H_2O).

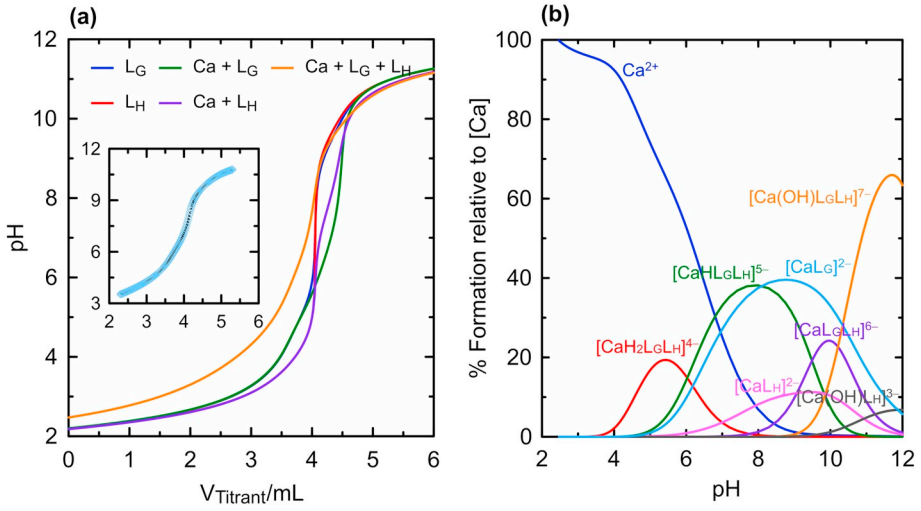

Fig. 4. (a) Real-time potentiometric titration curves for the protonation of L_G and L_H and the formation of the corresponding binary (M:L_G and M:L_H, 1:1) and ternary (M:L_G:L_H, 1:1:1) Ca^{2+} complexes. Inset: comparison of the theoretical (dashed line) and experimental (◊) titration data for the ternary mixtures (M:L_G:L_H, 1:1:1) at the complexation zone of the real-time potentiometric titration curve. (b) Speciation of the Ca^{2+} complexes in the ML_{mix} (L_{mix} = L_G + L_H; M:L_G:L_H, 1:1:1) system (I = 0.1 M; T = 25 °C; matrix, H_2O).

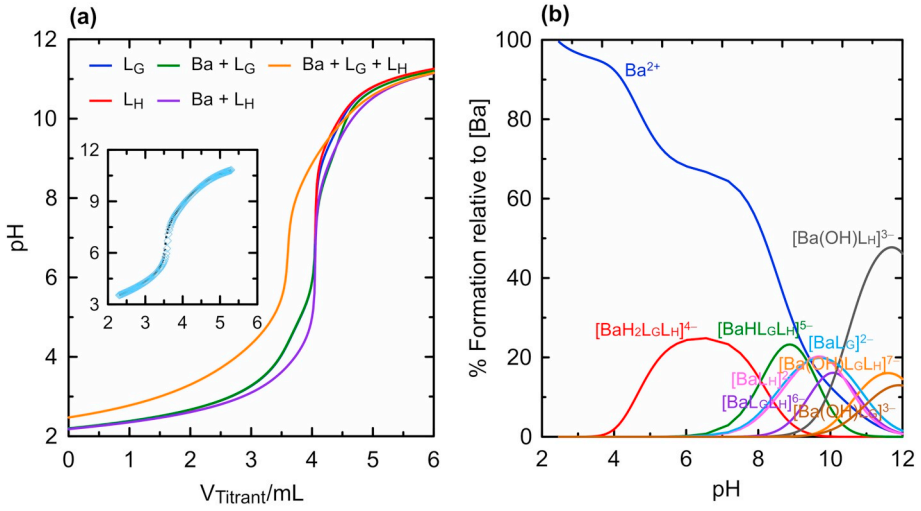

Fig. 5. (a) Real-time potentiometric titration curves for the protonation of L_G and L_H and the formation of the corresponding binary (M:L_G and M:L_H, 1:1) and ternary (M:L_G:L_H, 1:1:1) Ba^{2+} complexes. Inset: comparison of the theoretical (dashed line) and experimental (◊) titration data for the ternary mixtures (M:L_G:L_H, 1:1:1) at the complexation zone of the real-time potentiometric titration curve. (b) Speciation of the Ba^{2+} complexes in the ML_{mix} (L_{mix} = L_G + L_H; M:L_G:L_H, 1:1:1) system (I = 0.1 M; T = 25 °C; matrix, H_2O).

solutions, while the M^{2+} ions (Sr^{2+}, Mg^{2+}, Ca^{2+}, and Ba^{2+}) also compete to occupy the donor site resulting in the formation of protonated species. Hence, the formation of bi-protonated ($[MH_2L_GL_H]^{4-}$) species possibly occurred due to the dissociation of H^+ from the carboxyl positions of the chelators (pH ≥ 3.3; pK_a; L_G: 2.59, L_H: 2.14). The deprotonated ternary species ($[ML_GL_H]^{6-}$) started to form at ~pH 5.0, thereby indicating the coordination of M^{2+} with both the chelators via the amino nitrogen and carboxyl oxygen positions to probably generate five-membered chelate rings. The DFT-optimized plausible geometry of deprotonated ternary ML_{mix} complex of M^{2+} (Sr^{2+}, Mg^{2+}, Ca^{2+}, or Ba^{2+}) is shown in Fig. 7. A complex usually tend to possess minimal energy at the corresponding most stable state, which is indicated by the

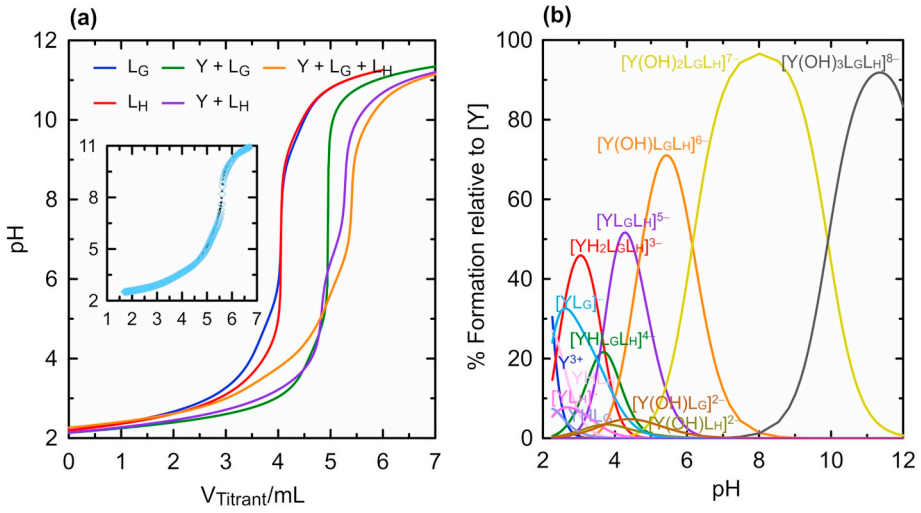

Fig. 6. (a) Real-time potentiometric titration curves for the protonation of L_G and L_H and the formation of the corresponding binary (M:L_G and M:L_H, 1:1) and ternary (M:L_G:L_H, 1:1:1) Y^{3+} complexes. Inset: comparison of the theoretical (dashed line) and experimental (◊) titration data for the ternary mixtures (M:L_G:L_H, 1:1:1) at the complexation zone of the real-time potentiometric titration curve. (b) Speciation of the Y^{3+} complexes in the ML_{mix} (L_{mix} = L_G + L_H; M:L_G:L_H, 1:1:1) system (I = 0.1 M; T = 25 °C; matrix, H_2O).

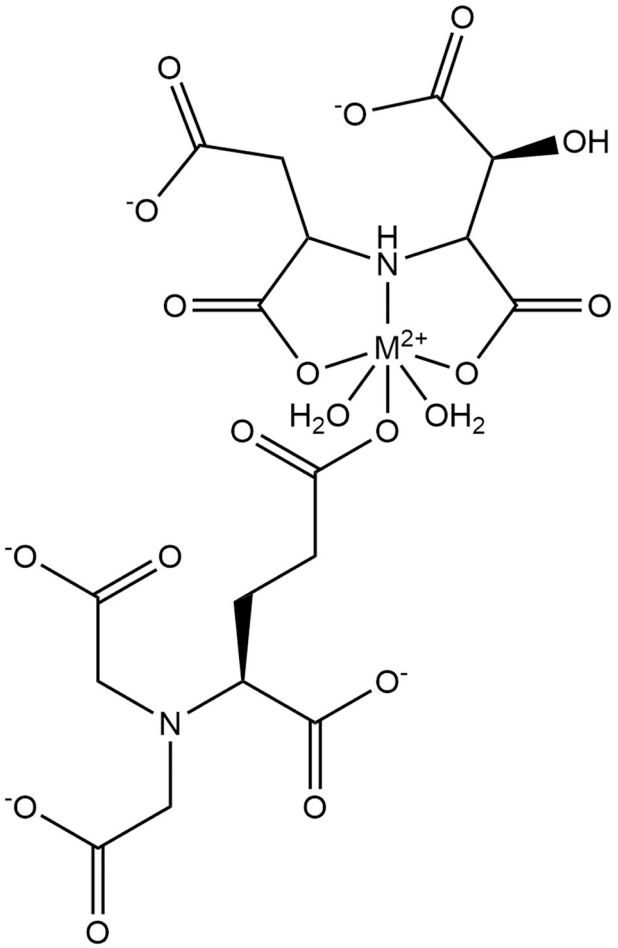

Fig. 7. Modeling of possible binding sites in the deprotonated ternary complex ($[ML_GL_H]^{6-}·2H_2O$; M = Sr^{2+}, Mg^{2+}, Ca^{2+}, or Ba^{2+}) using Gaussian 16W.

more negative values of Gibbs free energy of reaction (Δ_rG) [50]. The trend in relative stability of deprotonated ternary ML_{mix} complexes of M^{2+} was predicted in terms of the Δ_rG using the Gibbs free energy (G) of each DFT-optimized molecules (Table 2).

3.3. Trend in ternary complexation behavior

The overall formation constants ($\log_{10}\beta_{pqrs}$) of the Sr^{2+}, Mg^{2+}, Ca^{2+}, and Ba^{2+} ternary complexes in the ML_{mix} system are inversely correlated with the corresponding drift in atomic radius (pm): Mg^{2+} (145) < Ca^{2+} (194) < Sr^{2+} (219) < Ba^{2+} (253) [51,52]. However, the $\log_{10}\beta_{pqrs}$ values displayed a different trend: Mg^{2+} (9.08) < Ca^{2+} (9.43) > Sr^{2+} (7.67) > Ba^{2+} (7.17) (Fig. 8a). The atomic radius of Y^{3+} is 212 pm [52], while the ternary Y^{3+}–L_{mix} displays a much higher $\log_{10}\beta_{pqrs}$ value (25.26) than those of Sr^{2+}, Mg^{2+}, Ca^{2+}, and Ba^{2+}. Therefore, the atomic radius concept was considered inadequate for the comparison of the complexation behavior among the di- and trivalent cations.

The comparative formation order of the complexes in the ML_{mix} system can also be assumed using the EN_{sol} (solution-phase electronegativity) scale. The EN_{sol} concept correlates the nature of metal-chelator bonding in solution with the electronegativity of the metal ions for complexes with a chelator. The EN_{sol} values for the ions included in the study can thus be arranged in descending order: Y^{3+} (2.829) > Mg^{2+} (2.158) > Ca^{2+} (1.862) > Sr^{2+} (1.779) > Ba^{2+} (1.692) [53]. This order better corresponded to the higher $\log_{10}\beta_{pqrs}$ values of the Y^{3+}–L_{mix} complexes than those of the M^{2+}–L_{mix} ternaries, even though the $\log_{10}\beta_{pqrs}$ value of Ca^{2+}–L_{mix} differed from the descending periodic series trend for the divalent ions (Fig. 8b). The weaker coordination of Mg^{2+} with L_{mix} [54] or better adoption of the Ca^{2+} ions

Table 2
Calculated Gibbs free energy (G) of each metal (M) and chelator (L; L_G, GLDA and L_H, HIDS) in the simulated reaction system, and Gibbs free energy of reaction (Δ_rG) of the ternary ML_{mix} complexes (M = Sr^{2+}, Mg^{2+}, Ca^{2+}, or Ba^{2+}; L_{mix} = L_G + L_H, 1:1)[a,b].

Molecule	G/hartree	Δ_rG/hartree
Sr^{2+}	−30.334	
Mg^{2+}	−0.629	
Ca^{2+}	−36.441	
Ba^{2+}	−25.168	
L_G	−1005.414	
L_H	−1041.062	
$2H_2O$	−152.830	
$[SrL_GL_H]^{6-}·2H_2O$	−2229.801	−0.161
$[MgL_GL_H]^{6-}·2H_2O$	−2200.163	−0.228
$[CaL_GL_H]^{6-}·2H_2O$	−2235.942	−0.196
$[BaL_GL_H]^{6-}·2H_2O$	−2224.532	−0.058

[a] Calculation results from simulation by Gaussian 16W. Method: B3LYP. Basis sets: LanL2DZ (Sr^{2+}, Mg^{2+}, Ca^{2+}, or Ba^{2+}); 6-31 G(d) (C, N, O, and H); Solvation method: CPCM (solvent, H_2O). 1 hartree = 2.62 × 10^3 kJ mol^{-1}.

[b] Simulation assumptions include fully-deprotonated chelators, 1:1:1 interaction among the M^{2+}, L_G, and L_H, while the impact of background electrolyte and variation in matrix pH were ignored.

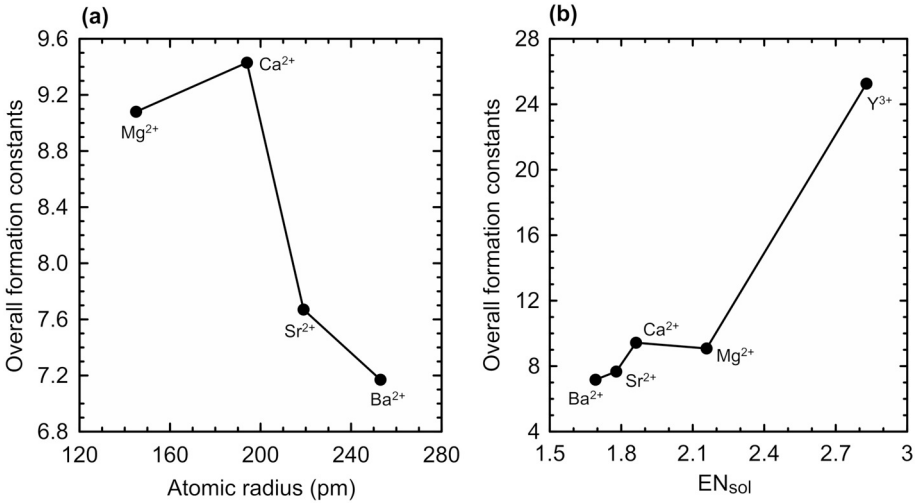

Fig. 8. Trends in the overall formation rate of the ternary Sr^{2+}, Mg^{2+}, Ca^{2+}, Ba^{2+}, and Y^{3} complexes in the ML_{mix} (L_{mix} = L_G + L_H; M:L_G:L_H, 1:1:1) system with the corresponding variations in (a) atomic radii of the elements and (b) solution-phase electronegativity (EN_{sol}) (I = 0.1 M; T = 25 °C; matrix, H_2O).

Table 3
Logarithms of the stability constants of the ternary ML_{mix} complexes (M = Sr^{2+}, Mg^{2+}, Ca^{2+}, Ba^{2+}, and Y^{3+}; L_{mix} = L_G + L_H, L_G, GLDA and L_H, HIDS)[a,b].

Metal	$\log\beta_{L_{mix}}$	$\log K_{ML_HL_G}$	$\log K_{ML_GL_H}$	$\log K_{ML_G}$	$\log K_{ML_H}$	$\Delta \log K$
Sr^{2+}	7.67 ± 0.04	2.97	3.63	4.04	4.70	−1.07
Mg^{2+}	9.08 ± 0.03	3.51	3.77	5.31	5.57	−1.80
Ca^{2+}	9.43 ± 0.01	4.38	3.55	5.88	5.05	−1.50
Ba^{2+}	7.17 ± 0.02	3.37	3.53	3.64	3.80	−0.27
Y^{3+}	25.26 ± 0.01	12.51	10.51	14.75	12.75	−2.24

[a] I = 0.1 M; T = 25 °C; M:L_G:L_H = 1:1:1; matrix, H_2O.
[b] Log$K$ values of the binary Sr^{2+}, Mg^{2+}, Ca^{2+}, Ba^{2+}, and Y^{3+} complexes with L_G and L_H (I = 0.1 M; T = 25 °C; M:L_G or M:L_H = 1:1; matrix, H_2O) was reported by Begum et al. [19].

within the stereo-configuration of L_{mix} [55,56] could be a reason for such 'irregular' behavior of Ca^{2+} in the $\log_{10}\beta_{pqrs}$ sequence in relation to the corresponding series of the atomic radius and EN_{sol} of the elements.

3.4. Relative stability of the ternary complexes

The coordination and oxidation characteristics of the metal and structural orientation of the chelator control the electrostatic and covalent-type interaction patterns among the components in the ML_{mix} system and determine the stability of the corresponding ternary complexes [57]. The relative stability of the ternary complexes in the ML_{mix} system, as compared to that of the corresponding binaries, can be quantitatively and most suitably expressed in terms of $\Delta\log K$ [29,45]. $\Delta\log K$ represents the difference between the complexation constants of the ternary and binary complexes; therefore, the derived $\Delta\log K$ is also a constant [49]:

$$\Delta \log K = \log K_{ML_HL_G} - \log K_{ML_G} = \log K_{ML_GL_H} - \log K_{ML_H} \quad (11)$$

The $\Delta\log K$ values for the ML_{mix} (M = Sr^{2+}, Mg^{2+}, Ca^{2+}, Ba^{2+}, and Y^{3+}; L_{mix} = L_G + L_H) system (Table 3) indicated the higher stabilities of the binary complexes over those of the corresponding ternaries. The pattern was generally attributed to the availability of more coordination positions to a metal ion for binding with the first chelator as compared to that of the second chelator [45,47]. However, it can also be assumed that the interaction of the component chelators with a metal ion was mutual and both chelators act together in their corresponding orientation with the same metal ion during the formation of ternary complexes in the ML_{mix} system [49]. The interaction scenario can be expressed as:

$$ML_G + ML_H \leftrightharpoons ML_GL_H + M \quad (12)$$

The formation pathway of the ternary complexes favor Eq. (12) if the experimentally derived $\Delta\log K$ value > −0.9 [49], as observed for the ternary complexation of Sr^{2+}, Mg^{2+}, Ca^{2+}, and Y^{3+}, but not for Ba^{2+}, with the L_{mix}.

The comparison of the real-time titration curves for the M:L_G or M:L_H (1:1) and M:L_G:L_H (1:1:1) systems indicated that deprotonation occurred at a higher pH for the 1:1 than for the 1:1:1 interactions (Figs. 2a, 3a, 4a, 5a, and 6a). Such a pattern also confirms the lower stabilities of the ternary complexes compared to those of the corresponding binaries; i.e., the $\Delta\log K$ values will be negative [48] due to the lack of interactions outside the coordination sphere [58].

The previously reported [20,59] higher order of stability of the ML complexes with trivalent ions over those with divalent ions has also been observed in this work (Table 3). This tendency is attributable to the differences in the corresponding ion size and charge that facilitate the stronger ionic binding of the trivalent ions, compared to that of the divalent ions, with the chelators [60].

4. Conclusion

The formation of ternary complexes with Sr^{2+}, Mg^{2+}, Ca^{2+}, Ba^{2+}, and Y^{3+} (M) and two biodegradable chelators (L_G and L_H) was analyzed using data from real-time potentiometric titrations (I = 0.10 M; T = 25 °C). The experimental potentiometric data obtained for M:L_G:L_H (1:1:1) suggested different behavior to that observed for the M:L_G and M:L_H (1:1) complexes. These data were fitted using different composition models to assess the relative proportion and possible speciation of the ternary complexes and to calculate the corresponding stability constants. The complexation trend of the ternary complexes was discussed in terms of cation ionic radii and EN_{sol}, and the specific behavior of Ca^{2+} was noted. The stability of the ternary complexes of L_G and L_H with the divalent ions (Sr^{2+}, Mg^{2+}, Ca^{2+}, and Ba^{2+}) was relatively lower than that of the trivalent Y^{3+}. Moreover, the relative stability of the ternary complexes was lower than that of the corresponding binary complexes. The context of this study was the recovery of radioisotopes and lanthanides from solid waste using eco-compliant chelators. Hence, the results reveal that in terms of element-binding capacity, L_G or L_H would be a better extractant than the mixed-chelators.

Abbreviations

GLDA or L_G	2-[bis(carboxymethyl)amino]pentanedioic acid
HIDS or L_H	2-(1,2-dicarboxyethylamino)-3-hydroxy-butanedioic acid
EDTA	2,2′,2″,2‴-(ethane-1,2-diyldinitrilo)tetraacetic acid
DTPA	2-[bis[2-[bis(carboxymethyl)amino]ethyl]amino]acetic acid
EDDS	2-[2-(1,2-dicarboxyethylamino)ethylamino]butanedioic acid
IDSA	2-(1,2-dicarboxyethylamino)butanedioic acid
MGDA	2-[bis(carboxymethyl)amino]propanoic acid
GLEE	glass electrode evaluation
HySS	Hyperquad simulation and speciation
G	Gibbs free energy
$\Delta_r G$	Gibbs free energy of reaction
EN_{sol}	solution-phase electronegativity

Acknowledgment

This work was supported by the (a) Grants-in-Aid for Scientific Research (17K00622, 18H03389, 18H03399) from the Japan Society for the Promotion of Science, (b) Science and Technology Research Partnership for Sustainable Development (SATREPS), Japan Science and Technology Agency (JST)/Japan International Cooperation Agency (JICA), and (c) Interdisciplinary Project on Environmental Transfer of Radionuclides (F-18-1, FY2018) in collaboration with the Center for Research in Isotopes and Environmental Dynamics, University of Tsukuba, Japan.

Appendix A. Supplementary data

Supplementary data to this article can be found online at https://doi.org/10.1016/j.jinorgbio.2019.03.018.

References

[1] N. Vajda, C.-K. Kim, Appl. Radiat. Isot. 68 (2010) 2306–2326.
[2] C.F.V. Mason, N. Lu, J. Conca, S.S. Hecker, C.F.V. Mason, K.K. Kadyrzhanov, S.B. Kislitsin (Eds.), Nuclear Physical Methods in Radioecological Investigations of Nuclear Test Sites, Springer, Dordrecht, Netherlands, 2000, pp. 89–97.
[3] M. Herranz, R. Idoeta, F. Legarda, Radiat. Meas. 46 (2011) 680–686.
[4] L.M. Kagan, V.B. Kadatsky, J. Environ. Radioact. 33 (1996) 27–39.
[5] G. Arapis, E. Petrayev, E. Shagalova, O. Zhukova, G. Sokolik, T. Ivanova, J. Environ. Radioact. 34 (1997) 171–185.
[6] E. Shagalova, O. Zhukova, M. Germenchuk, I. Matveenko, Z. Bakarikova, J. Radioanal. Nucl. Ch. 246 (2000) 521–525.
[7] US EPA, Radionuclide Basics: Strontium-90, https://www.epa.gov/radiation/radionuclide-basics-strontium-90, (2017) , Accessed date: 3 November 2018.
[8] US NRC, NRC Glossary: Bone Seeker, https://www.nrc.gov/reading-rm/basic-ref/glossary/bone-seeker.html, (2018) , Accessed date: 3 November 2018.
[9] B. Nowack, Environ. Sci. Technol. 36 (2002) 4009–4016.
[10] J.L. Means, D.A. Crerar, J.O. Duguid, Science 200 (1978) 1477–1481.
[11] S. Fukuda, Curr. Med. Chem. 12 (2005) 2765–2770.
[12] H. Sawai, I.M.M. Rahman, C. Lu, Z.A. Begum, M. Saito, H. Hasegawa, Microchem. J. 134 (2017) 230–236.
[13] Z.A. Begum, I.M.M. Rahman, H. Sawai, H. Hasegawa, H. Hasegawa, I.M.M. Rahman, M.A. Rahman (Eds.), Environmental Remediation Technologies for Metal-Contaminated Soils, Springer, Tokyo, Japan, 2016, pp. 197–218.
[14] A. Ferraro, M. Fabbricino, E.D. van Hullebusch, G. Esposito, F. Pirozzi, Rev. Environ. Sci. Biotechnol. 15 (2016) 111–145.
[15] G. Dermont, M. Bergeron, G. Mercier, M. Richer-Laflèche, J. Hazard. Mater. 152 (2008) 1–31.
[16] I.M.M. Rahman, M.M. Hossain, Z.A. Begum, M.A. Rahman, H. Hasegawa, I.A. Golubev (Ed.), Handbook of Phytoremediation, Nova Science Publishers, Hauppauge, NY, USA, 2010, pp. 709–722.
[17] S. Tandy, K. Bossart, R. Mueller, J. Ritschel, L. Hauser, R. Schulin, B. Nowack, Environ. Sci. Technol. 38 (2004) 937–944.
[18] L. Zhang, Z. Zhu, R. Zhang, C. Zheng, H. Zhang, Y. Qiu, J. Zhao, J. Environ. Sci. 20 (2008) 970–974.
[19] Z.A. Begum, I.M.M. Rahman, H. Hasegawa, J. Mol. Liq. 242 (2017) 1123–1130.
[20] Z.A. Begum, I.M.M. Rahman, H. Sawai, Y. Tate, T. Maki, H. Hasegawa, J. Chem. Eng. Data 57 (2012) 2723–2732.
[21] Z.A. Begum, I.M.M. Rahman, Y. Tate, Y. Egawa, T. Maki, H. Hasegawa, J. Solut. Chem. 41 (2012) 1713–1728.
[22] Z.A. Begum, I.M.M. Rahman, H. Sawai, S. Mizutani, T. Maki, H. Hasegawa, Water Air Soil Pollut. 224 (2013) 1381.
[23] H. Hasegawa, Z.A. Begum, R. Murase, K. Ishii, H. Sawai, A.S. Mashio, T. Maki, I.M.M. Rahman, Waste Manag. 80 (2018) 17–25.
[24] H. Sawai, I.M.M. Rahman, Y. Tsukagoshi, T. Wakabayashi, T. Maki, S. Mizutani, H. Hasegawa, Chem. Eng. J. 277 (2015) 219–228.
[25] Z.A. Begum, I.M.M. Rahman, Y. Tate, H. Sawai, T. Maki, H. Hasegawa, Chemosphere 87 (2012) 1161–1170.
[26] A.E. Angkawijaya, A.E. Fazary, E. Hernowo, M. Taha, Y.-H. Ju, J. Chem. Eng. Data 56 (2011) 532–540.
[27] Y. Marcus, I. Eliezer, Coordin. Chem. Rev. 4 (1969) 273–322.
[28] A.A. El-Sherif, M.M. Shoukry, R. van Eldik, Dalton Trans. (2003) 1425–1432.
[29] M.M. Shoukry, P. Indian AS-Chem. Sci. 102 (1990) 19–24.
[30] W. Madden, L. Hernández, A. Pérez, E. Del Carpio, V. Lubes, J. Mol. Liq. 221 (2016) 88–92.
[31] B. Veera Swami, P. Bhushanavathi, G. Nageswara Rao, U. Viplava Prasad, P. Natl. A. Sci. India A 82 (2012) 283–289.
[32] W. Dong, S.C. Brooks, Environ. Sci. Technol. 40 (2006) 4689–4695.
[33] I.T. Ahmed, J. Chem. Eng. Data 48 (2003) 272–276.
[34] X. Guo, G. Zhang, Z. Wei, L. Zhang, Q. He, Q. Wu, T. Qian, J. Soils Sediments 18 (2018) 835–844.
[35] R. Qiu, Z. Zou, Z. Zhao, W. Zhang, T. Zhang, H. Dong, X. Wei, J. Soils Sediments 10 (2010) 45–53.
[36] A. Kabata-Pendias, Trace Elements in Soils and Plants, 4th edn, CRC Press, Boca Raton, FL, 2010.
[37] A. Jeske, Soil Sci. Ann. 64 (2013) 2–7.
[38] H. Tsukada, A. Takeda, T. Takahashi, H. Hasegawa, S. Hisamatsu, J. Inaba, J. Environ. Radioact. 81 (2005) 221–231.
[39] B. Kř'ibek, J. Podlaha, Org. Geochem. 2 (1980) 93–97.
[40] P. Gans, B. O'Sullivan, Talanta 51 (2000) 33–37.
[41] L. Alderighi, P. Gans, A. Ienco, D. Peters, A. Sabatini, A. Vacca, Coordin. Chem. Rev. 184 (1999) 311–318.
[42] P. Gans, A. Sabatini, A. Vacca, Talanta 43 (1996) 1739–1753.
[43] C.F. Baes, R.E. Messmer, The Hydrolysis of Cations, Wiley Interscience, NY, USA, 1976.
[44] Gaussian 16, Rev. A.03. Wallingford, CT, USA, 2016.
[45] R.B. Martin, R. Prados, J. Inorg. Nucl. Chem. 36 (1974) 1665–1670.
[46] S.S. Jones, F.A. Long, J. Phys. Chem. 56 (1952) 25–33.
[47] R. Griesser, H. Sigel, Inorg. Chem. 9 (1970) 1238–1243.
[48] R. Griesser, H. Sigel, Inorg. Chem. 10 (1971) 2229–2232.
[49] H. Sigel, Angew. Chem. Int. Edit. 14 (1975) 394–402.
[50] G. Frison, G. Ohanessian, J. Comput. Chem. 29 (2008) 416–433.
[51] E. Clementi, D.L. Raimondi, J. Chem. Phys. 38 (1963) 2686–2689.
[52] E. Clementi, D.L. Raimondi, W.P. Reinhardt, J. Chem. Phys. 47 (1967) 1300–1307.
[53] K. Li, M. Li, D. Xue, J. Phys. Chem. A 116 (2012) 4192–4198.
[54] E.T. Clarke, A.E. Martell, Inorg. Chim. Acta 190 (1991) 27–36.
[55] R. Aruga, Inorg. Chem. 19 (1980) 2895–2896.
[56] R.J. Motekaitis, A.E. Martell, Inorg. Chem. 28 (1989) 3499–3503.
[57] C.F. Bell, Principles and Applications of Metal Chelation, Clarendon Press, Oxford, UK, 1977.
[58] P. Bhushanavathi, B. Veeraswami, G. Nageswara Rao, P. Natl. A. Sci. India A 83 (2013) 299–307.
[59] E.G. Vinokurov, V.V. Bondar, Russ. J. Coord. Chem. + 29 (2003) 66–72.
[60] N. Raos, A. Milièevic, D.A. Morrison (Ed.), Handbook of Inorganic Chemistry Research, Nova Science Publishers, Hauppauge, NY, USA,, 2011, pp. 267–294.